

## Transition strengths in $^{79}\text{Rb}$

J. W. Holcomb, J. Döring, T. Glasmacher, G. D. Johns,  
T. D. Johnson, M. A. Riley, P. C. Womble, and S. L. Tabor

*Department of Physics, Florida State University, Tallahassee, Florida 32306*

(Received 26 March 1993)

High angular momentum states in  $^{79}\text{Rb}$  were populated via the  $^{63}\text{Cu}(^{19}\text{F},2pn)^{79}\text{Rb}$  and  $^{65}\text{Cu}(^{18}\text{O},4n)^{79}\text{Rb}$  reactions. The 65 MeV  $^{19}\text{F}$  and 65 MeV  $^{18}\text{O}$  beams were provided by the Florida State University FN Tandem accelerator. Prompt  $\gamma$ - $\gamma$  coincidences were measured for both reactions. Two additional  $\gamma$  cascades have been assigned to  $^{79}\text{Rb}$ , including a new high-excitation structure dominated by dipole transitions. Firm spin assignments were made for the first time for a number of states by means of directional correlation ratios and an angular distribution measurement using the  $^{63}\text{Cu}(^{19}\text{F},2pn)$  reaction. The Doppler-shift attenuation method was used to determine lifetimes for states and their respective side-feeding times in both the yrast positive-parity and yrast negative-parity states. Transition quadrupole moments were deduced from the transition strengths and compared with those predicted by Woods-Saxon cranking calculations. The energy spacings and mixing ratios were compared with particle-rotor calculations.

PACS number(s): 21.10.Tg, 23.20.-g, 27.50.+e

### I. INTRODUCTION

It has been demonstrated in recent years that the shapes of  $\gamma$ -soft even-even nuclei are greatly affected when an odd nucleon is added to the system. Shape polarization in many odd- $A$  nuclei in the mass 80 region is expected to be highly dependent on the single-particle orbital occupied by the odd nucleon. The present study of  $^{79}\text{Rb}$  has been carried out in order to investigate shape polarization due to an odd proton.

$^{79}\text{Rb}$  is of particular interest because, with  $N = 42$ , it lies at the border of the well-deformed highly rotational region which includes  $^{77}\text{Rb}$  [1] and the moderately deformed  $\gamma$ -soft region including  $^{81}\text{Rb}$  [2]. For  $^{77}\text{Rb}$ , the transition quadrupole moments,  $Q_t$ , average 3.1 (3.5) eb in the lowest positive-parity (negative-parity) band, corresponding to very large axially symmetric deformations of  $\beta_2 \approx 0.45$ . Conversely, a moderate deformation was seen in  $^{81}\text{Rb}$  [2], with transition quadrupole moments ranging from 2.0 to 2.5 eb and corresponding axial deformations of  $\beta_2 \approx 0.3$ .

Using a Woods-Saxon potential in a cranking model, a theoretical analysis [3] of the positive-parity rotational bands of  $^{79}\text{Rb}$  has predicted  $Q_t$  values of approximately 3.0 eb for positive-parity states and slightly higher for those of negative parity. This follows the general trend of nuclear deformations in this region [4].

The present experiment was undertaken to study the deformation of  $^{79}\text{Rb}$  by measuring the mean lifetimes of states and to explore the structure of sidebands. A recent investigation [5] of the high-spin level scheme of  $^{79}\text{Rb}$  has shown good rotational behavior and alignment properties deduced from the energy spacings up to a spin of  $\frac{41}{2}$  in bands of both parities. An earlier study [6] determined mean lifetimes of the states up to spins of  $\frac{21}{2}^-$  and  $\frac{25}{2}^+$ . In the present work lifetimes were measured for higher-lying levels in the rotational bands by using an array of five Compton-suppressed Ge detectors. These lifetimes provide a good test of the nuclear deformations

predicted by Hartree-Fock-Bogolyubov cranking calculations. It was also possible to determine side-feeding times by analyzing the line shapes in spectra in coincidence with transitions above the state of interest.

Other goals of this work were to make firm spin assignments from directional correlation ratios and angular distributions, to verify the assignment [5] of another band structure to  $^{79}\text{Rb}$ , and to look for evidence for a high-lying 3-quasiparticle (qp) band which had been seen in  $^{83}\text{Rb}$  [7],  $^{81}\text{Rb}$  [8, 9],  $^{77}\text{Br}$  [10],  $^{79}\text{Br}$  [11], and  $^{81}\text{Br}$  [12]. This band is characterized by strong  $\Delta I = 1$  transitions. Decays out of these high-lying bands occur with about equal intensity to low-lying states of both parities.

### II. EXPERIMENTAL TECHNIQUES

High-spin states of  $^{79}\text{Rb}$  were studied via the  $^{63}\text{Cu}(^{19}\text{F},2pn)$  and  $^{65}\text{Cu}(^{18}\text{O},4n)$  fusion-evaporation reactions. The 65 MeV  $^{19}\text{F}$  and 65 MeV  $^{18}\text{O}$  beams were provided by the Florida State University Tandem accelerator. The  $^{63}\text{Cu}$  target was enriched to 99.89% with a thickness of 14.51 mg/cm<sup>2</sup> and the  $^{65}\text{Cu}$  target was a self-supporting foil with a thickness of 0.6 mg/cm<sup>2</sup> enriched to 99%.

For the first reaction, both  $\gamma$ - $\gamma$  coincidences and angular distributions were measured. Five bismuth germanate (BGO) Compton-suppressed high-purity Ge detectors were used to collect the  $\gamma$ - $\gamma$  coincidences. Four were placed at 90° with respect to the beam direction while the fifth was placed at a 6° angle. The forward detector was placed to allow measurements of lifetimes of the short-lived states via the Doppler-shift attenuation method (DSAM). More than 650 million coincidences were recorded on high-density VHS tapes for subsequent analysis. Internal energy calibrations were made using a least-squares fitting of the following  $\gamma$ -ray energies (in keV) to a linear function of channel number: 197.15 ( $^{19}\text{F}$ ), 454.9 ( $^{78}\text{Kr}$ ), 511.0 ( $e^+e^-$ ), 669.6, and 1327.0

( $^{63}\text{Cu}$ ). The coincidence events between any two of the four  $90^\circ$  detectors were then gainshifted to a dispersion of 0.8 keV/channel and sorted [13] into a 2500 channel triangular array on a RIDGE3200 computer. The coincidences between the  $6^\circ$  and any one of the  $90^\circ$  detectors were similarly gainshifted and sorted into a  $2500 \times 2500$  channel square array.

Angular distributions were measured using two Compton-suppressed Ge detectors. One detector was moved to angles of  $90^\circ$ ,  $70^\circ$ ,  $45^\circ$ ,  $20^\circ$ , and  $0^\circ$  with respect to the beam axis while the monitor detector remained fixed at  $90^\circ$ . The yields were normalized to the intensities recorded by a fixed-angle monitor detector.

In the  $^{65}\text{Cu}(^{18}\text{O},4n)$  experiment, the Pitt-FSU detector array [14], with nine Compton-suppressed Ge detectors in operation at the time, was used to collect approximately 180 million coincidence events. Two detectors were positioned at  $35^\circ$ , three at  $90^\circ$  and four at  $145^\circ$  with respect to the beam direction. Internal energy calibrations automatically corrected for the Doppler shifts of the  $\gamma$  rays due to recoils escaping the thin target. The data were sorted into a 2500 channel triangular array on a DECstation 5000/200 computer for off-line analysis.

The transition energies observed in the two reactions agreed rather well with each other and with several earlier works [6, 15], but are consistently 1–2 keV higher than those reported in Ref. [5].

### III. THE LEVEL SCHEME

The level scheme of  $^{79}\text{Rb}$  shown in Fig. 1 was deduced from coincidence spectra generated by gating on the two-dimensional arrays. In most cases it is in agreement with previously published level schemes [5, 6]. The emphasis in the present work was on lifetime measurements and sideband structures. States of somewhat higher spin are known from a previous work [5].

Angular distribution measurements and directional correlation of oriented nuclei (DCO) ratios from spectra generated from the square array provided a means of deducing the multipolarity of the transitions. DCO ratios were calculated wherever possible according to

$$R_{\text{DCO}} = \frac{I_\gamma \text{ (at } 6^\circ \text{ gated by } \gamma_G \text{ at } 90^\circ)}{I_\gamma \text{ (at } 90^\circ \text{ gated by } \gamma_G \text{ at } 6^\circ)} \quad (1)$$

with the coincidence gate  $\gamma_G$  always from one or more of the  $E2$  transitions. Stretched  $E2$  transitions are expected to yield DCO ratios of approximately 1, while, depending on the multipole mixing ratio,  $\Delta I = 1$  transitions yield DCO ratios ranging from 0 to 2. If the mixing ratios are small, the DCO ratios for  $\Delta I = 1$  transitions are expected [16] to be near 0.5. DCO ratios obtained from the  $^{63}\text{Cu}(^{19}\text{F},2pn)$  reaction are listed in Table I.

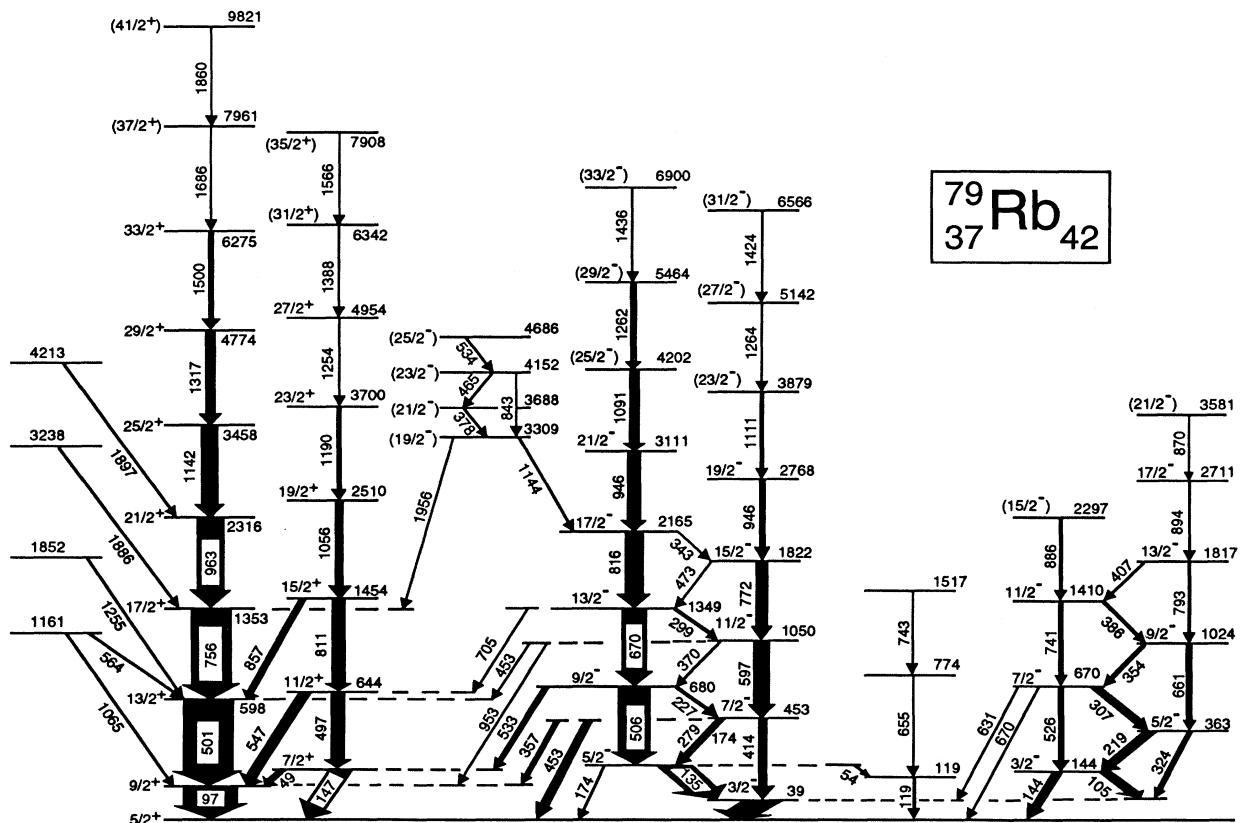


FIG. 1. The level scheme of  $^{79}\text{Rb}$  as deduced from the present work. The widths of the lines are approximately proportional to the transition intensities. Note that a nonlinear energy ordinate is used to better display the low energy portion of the level scheme. The vertical displacement is proportional to  $(E_{\text{level}})^{2/3}$ .

TABLE I. Energies, relative intensities, DCO ratios, and multipolarities for transitions in  $^{79}\text{Rb}$ .

$E_{\text{lev}}$ (keV)	$E_{\gamma}$ (keV)	$I_i \rightarrow I_f$	$I_{\gamma}$	$R_{\text{DCO}}$
96.7	96.7(1)	$9/2^+ \rightarrow 5/2^+$		0.97(6)
147.0	147.0(1)	$7/2^+ \rightarrow 5/2^+$	35(2)	1.48(8)
	50.0(10)	$7/2^+ \rightarrow 9/2^+$		
597.5	500.8(1)	$13/2^+ \rightarrow 9/2^+$	100(1)	0.99(4)
643.9	496.9(1)	$11/2^+ \rightarrow 7/2^+$	20(2)	1.15(5)
	547.2(1)	$11/2^+ \rightarrow 9/2^+$	15(1)	1.50(14)
1353.2	755.7(1)	$17/2^+ \rightarrow 13/2^+$	79(3)	1.02(5)
1454.4	810.5(1)	$15/2^+ \rightarrow 11/2^+$	22(1)	1.00(10)
	856.9(3)	$15/2^+ \rightarrow 13/2^+$	7(2)	
2315.7	962.5(1)	$21/2^+ \rightarrow 17/2^+$	56(2)	1.02(5)
2510.2	1055.8(1)	$19/2^+ \rightarrow 15/2^+$	12(1)	1.08(12)
3457.5	1141.8(1)	$25/2^+ \rightarrow 21/2^+$	32(3)	1.01(9)
3699.8	1189.6(4)	$23/2^+ \rightarrow 19/2^+$	6(2)	1.03(15)
4774.3	1316.8(3)	$29/2^+ \rightarrow 25/2^+$	15(3)	0.96(17)
4954.2	1254.4(4)	$27/2^+ \rightarrow 23/2^+$	4(2)	0.95(14)
6274.5	1500.2(5)	$33/2^+ \rightarrow 29/2^+$	6(2)	0.93(17)
6342.3	1388.1(9)	$(31/2^+) \rightarrow 27/2^+$	< 2	
7908.3	1566.0(12)	$(35/2^+) \rightarrow (31/2^+)$	< 2	
7960.8	1686.3(10)	$(37/2^+) \rightarrow 33/2^+$	< 2	
9820.8	1860.0(20)	$(41/2^+) \rightarrow (37/2^+)$	< 2	
1161.3	563.8(2)	$(13/2^+) \rightarrow 13/2^+$	< 2	0.29(5)
	1064.6(4)	$(13/2^+) \rightarrow 9/2^+$	5(1)	
1852.1	1254.6(3)	$(15/2^+) \rightarrow 13/2^+$	2(1)	0.25(3)
3239.2	1886.0(15)	$\rightarrow 17/2^+$	3(1)	
4213.0	1897.3(20)	$\rightarrow 21/2^+$	4(1)	
174.1	54.0(5)	$5/2^- \rightarrow$		
	174.1(3)	$5/2^- \rightarrow 5/2^+$	3(1)	
	135.1(2)	$5/2^- \rightarrow 3/2^-$	35(2)	0.21(3)
453.3	414.3(1)	$7/2^- \rightarrow 3/2^-$	13(1)	1.09(6)
	279.2(1)	$7/2^- \rightarrow 5/2^-$	12(2)	0.19(5)
	356.6(1)	$7/2^- \rightarrow 9/2^+$	8(1)	
	453.3(4)	$7/2^- \rightarrow 5/2^+$	13(4)	
679.9	505.8(1)	$9/2^- \rightarrow 5/2^-$	60(1)	1.04(6)
	226.6(2)	$9/2^- \rightarrow 7/2^-$	8(1)	0.15(4)
	532.9(2)	$9/2^- \rightarrow 7/2^+$	11(2)	
1050.1	596.8(1)	$11/2^- \rightarrow 7/2^-$	31(2)	0.93(8)
	370.2(2)	$11/2^- \rightarrow 9/2^-$	3(1)	0.11(4)
	953.4(3)	$11/2^- \rightarrow 9/2^+$	4(1)	
	453.9(4)	$11/2^- \rightarrow 13/2^+$	3(1)	
1349.4	669.5(1)	$13/2^- \rightarrow 9/2^-$	47(1)	0.96(4)
	299.3(1)	$13/2^- \rightarrow 11/2^-$	5(1)	0.23(5)
	705.1(3)	$13/2^- \rightarrow 11/2^+$	4(1)	
1822.1	772.0(1)	$15/2^- \rightarrow 11/2^-$	23(1)	0.86(10)
	472.7(2)	$15/2^- \rightarrow 13/2^-$	3(1)	
2165.1	815.7(1)	$17/2^- \rightarrow 13/2^-$	34(2)	1.03(5)
	343.0(2)	$17/2^- \rightarrow 15/2^-$	< 2	
2767.8	945.7(2)	$19/2^- \rightarrow 15/2^-$	8(2)	0.86(20)
3111.4	946.3(2)	$21/2^- \rightarrow 17/2^-$	18(2)	0.93(7)
3878.9	1111.1(4)	$(23/2^-) \rightarrow 19/2^-$	6(1)	
4202.0	1090.6(2)	$(25/2^-) \rightarrow 21/2^-$	14(2)	0.95(12)
5142.4	1263.5(5)	$(27/2^-) \rightarrow (23/2^-)$	3(1)	
5463.9	1261.9(5)	$(29/2^-) \rightarrow (25/2^-)$	13(2)	0.84(16)
6566.0	1423.6(10)	$(31/2^-) \rightarrow (27/2^-)$	< 2	
6900.3	1436.4(10)	$(33/2^-) \rightarrow (29/2^-)$	< 2	
39.0	39.0(10)	$3/2^- \rightarrow 5/2^+$		
143.7	104.7(2)	$3/2^- \rightarrow 3/2^-$	15(1)	0.97(14)
	143.7(15)	$3/2^- \rightarrow 5/2^+$	18(4)	0.63(15)

TABLE I. (Continued).

$E_{\text{lev}}$ (keV)	$E_{\gamma}$ (keV)	$I_i \rightarrow I_f$	$I_{\gamma}$	$R_{\text{DCO}}$
362.7	219.0(1)	$5/2^- \rightarrow 3/2^-$	34(2)	0.75(11)
	323.7(2)	$5/2^- \rightarrow 3/2^-$	6(1)	0.96(11)
669.7	526.0(1)	$7/2^- \rightarrow 3/2^-$	14(2)	1.07(14)
	307.0(1)	$7/2^- \rightarrow 5/2^-$	26(3)	0.76(10)
	630.7(3)	$7/2^- \rightarrow 3/2^-$	5(1)	
	669.7(3)	$7/2^- \rightarrow 5/2^+$	8(1)	
1024.0	661.3(1)	$9/2^- \rightarrow 5/2^-$	14(2)	1.03(28)
	354.3(1)	$9/2^- \rightarrow 7/2^-$	12(2)	0.72(8)
1410.2	740.5(1)	$11/2^- \rightarrow 7/2^-$	11(2)	0.99(11)
	386.2(2)	$11/2^- \rightarrow 9/2^-$	4(1)	0.85(14)
1816.7	792.7(2)	$13/2^- \rightarrow 9/2^-$	6(1)	0.99(11)
	406.5(2)	$13/2^- \rightarrow 11/2^-$	2(1)	0.51(10)
	2296.5	$(15/2^-) \rightarrow 11/2^-$	12(2)	
2710.8	894.1(5)	$17/2^- \rightarrow 13/2^-$	4(1)	1.10(7)
3581	870(5)	$(21/2^-) \rightarrow 17/2^-$	2(1)	
3309.4	1956.2(5)	$(19/2^-) \rightarrow 17/2^+$	< 2	
	1144.3(5)	$(19/2^-) \rightarrow 17/2^-$	< 2	
3687.5	378.1(2)	$(21/2^-) \rightarrow (19/2^-)$	< 2	
4152.2	842.8(3)	$(23/2^-) \rightarrow (19/2^-)$	< 2	
	464.7(2)	$(23/2^-) \rightarrow (21/2^-)$	< 2	
4686.4	534.2(2)	$(25/2^-) \rightarrow (23/2^-)$	< 2	
119.5	119.5(2)	$\rightarrow 5/2^+$	4(1)	
774.3	654.8(3)		< 2	
1517.2	742.9(4)		< 2	

In the analysis [17] of the experimental angular distribution data the distribution of magnetic substates was assumed to be Gaussian with a width of  $\sigma = 1$ . Curves of  $\chi^2$  were generated from a comparison of the experimental data with theoretical angular distributions assuming values of the mixing ratio ranging from  $\arctan(\delta) = -90^\circ$  to  $+90^\circ$ .

#### A. Positive-parity band

The spin of the ground state of  $^{79}\text{Rb}$  was determined to be  $\frac{5}{2}$  from an atomic-beam magnetic resonance measurement [18], and positive parity was established by the observation [19] of an allowed  $\beta$  decay branch to the 688 keV  $\frac{3}{2}^+$  state in  $^{79}\text{Kr}$ . Clements *et al.* [15] first assigned an  $E2$   $\gamma$ -ray sequence to  $^{79}\text{Rb}$  decaying from a  $(\frac{21}{2}^+)$  state and terminating into the  $\frac{5}{2}^+$  ground state. Two subsequent investigations [5, 6] extended this signature  $\alpha = +\frac{1}{2}$  band up to a  $(\frac{41}{2}^+)$  state, with angular distributions providing spin assignments up to the  $\frac{25}{2}^+$  state. In the present work, DCO ratios ranging from 0.93 to 1.02 for this sequence not only supported the previous spin assignments but also provided firm assignments up to the  $\frac{33}{2}^+$  state. Figure 2 shows the sum of coincidence spectra gated on the strong transitions in this cascade. The 1860 keV line was seen clearly only in the thin-target experiment, not shown here.

The signature  $\alpha = -\frac{1}{2}$  band is also known [5, 6] in  $^{79}\text{Rb}$  up to a spin of  $\frac{35}{2}$ . There is, however, a contradiction in the placement of the band relative to the  $\alpha = +\frac{1}{2}$

band. The earlier experiment [6] assigned an  $(\frac{11}{2}^+)$  state at 593.8 keV which decays by a 497.1 keV transition to the  $\frac{9}{2}^+$  state and by a 547.1 keV line to a state below the  $\frac{9}{2}^+$  level. The later experiment [5] assigned an  $(\frac{11}{2}^+)$  state at 642.8 keV which decays by a 497 keV transition to the  $(\frac{7}{2}^+)$  state and by a 547 keV line to the  $\frac{9}{2}^+$  level.

The latter placement of the  $\alpha = -\frac{1}{2}$  band is supported in the present work. Figure 3 shows a portion of the background-corrected spectrum in coincidence with the 97 keV transition. A clear coincidence is observed between the 547 keV transition and the 97 keV line from the  $\frac{9}{2}^+$  state, in contradiction to the earlier placement. Furthermore, a weak 49 keV transition is observed in coincidence with the 97 keV line, consistent with its placement between the 147 and 97 keV levels. A 147 keV transition is also clearly observed in the coincidence spectra gated on lines in the  $\alpha = -\frac{1}{2}$  band, consistent with its placement between the  $\frac{7}{2}^+$  level and the  $\frac{5}{2}^+$  ground state. The relative position of the signature  $\alpha = -\frac{1}{2}$  band with respect to the favored band ( $\alpha = +\frac{1}{2}$ ) is also supported by the observed 857 keV line between the  $\frac{15}{2}^+$  and  $\frac{13}{2}^+$  states.

No firm spin assignments for the  $\alpha = -\frac{1}{2}$  sequence had been previously established. From spectra obtained by adding the 497, 811, and 1056 keV gates, DCO ratios of approximately 1.5 were obtained for the 147 and 547 keV transitions (see Table I). This would imply a  $\Delta I = 1$  multipolarity for both transitions with negative mixing ratios [17]. An angular distribution was measured

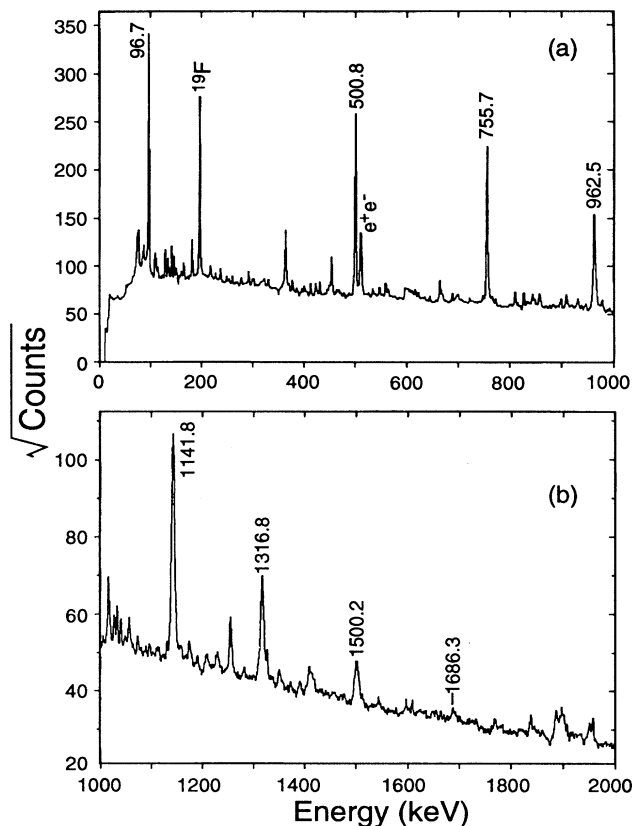


FIG. 2. Sum of  $90^\circ$  spectra gated on the 97, 501, 756, and 1142 keV transitions in the favored signature of the positive-parity band from the  $^{63}\text{Cu}(^{19}\text{F}, 2pn)^{79}\text{Rb}$  reaction.

to confirm these results. The results of this measurement can be found in Table II. Figure 4 shows curves of  $\chi^2$  versus the mixing ratio  $\delta$  for the 147 keV transition. The solid (dashed) line represents  $\chi^2$  for mixed  $M1/E2$  ( $E2/M3$ ) decay. Dipole character is clearly established with  $\delta = \tan(-11^\circ) = -0.19$ , in good agreement with the DCO ratio. This establishes a spin and parity of  $\frac{7}{2}^+$  for its parent state. Likewise, the angular distribution measurement of the 547 keV transition is consistent with dipole character with a mixing ratio of  $\delta = \tan(-21^\circ) = -0.38$ , thus assigning the  $\frac{11}{2}^+$  spin and parity. DCO ratios ranged from 0.95 to 1.08 for the  $\Delta I = 2$  transitions in the decays from the  $\frac{27}{2}^+$  to the  $\frac{7}{2}^+$  states. Due to lack of statistics, no DCO ratio could be measured for the 1388 and 1566 keV transitions. Firm spin assignments are, therefore, established up to a spin of  $\frac{27}{2}^+$ .

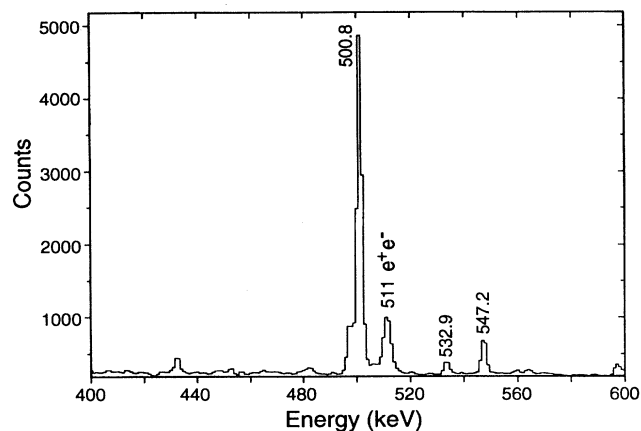


FIG. 3. A portion of the  $\gamma$  spectrum in coincidence with the 97 keV transition.

### B. States decaying into the positive-parity band

Four states at 1161, 1852, 3239, and 4213 keV are shown decaying into positive-parity states on the left side of Fig. 1. Only a single transition was seen from each state, except for the lowest one, but the coincidence relations are clear. No decays were seen between the states, so it is not clear that this group of states forms a collective band.

### C. Yrast negative-parity states

A pair of complementary signature negative-parity bands based on the 39 keV state is also known [5, 6] up to  $(\frac{35}{2}^-)$  and  $(\frac{41}{2}^-)$ . In the present work several new  $E1$  transitions were seen from this band to the positive-parity band, as well as, three previously unreported intraband  $\Delta I = 1$  transitions extending up to the 2165 keV  $\frac{17}{2}^-$  state. The measurement of DCO ratios has permitted spin assignments for the states up to  $\frac{21}{2}^-$ . Transitions having DCO ratios ranging from 0.84 to 1.09 were assigned  $\Delta I = 2$ . DCO ratios for the  $M1/E2$  mixed transitions were all below 0.30, implying a substantial positive mixing ratio. Due to lack of statistics, no DCO ratios could be determined for the 343.0, 472.7, 1111.1, 1261.9, 1263.5, 1423.6, and 1436.4 keV transitions.

Spin assignments in these bands are based on the spin and parity of the 39 keV bandhead which was previously tentatively assigned [5]  $(\frac{3}{2}^-)$ . The observation of allowed  $\beta$  decay [20, 21] to this state from the  $\frac{3}{2}^-$  ground state [22, 23] of  $^{79}\text{Sr}$  limits its spin and parity to  $\frac{1}{2}^-$ ,  $\frac{3}{2}^-$ , or  $\frac{5}{2}^-$ . If

TABLE II. Angular distribution coefficients and mixing ratios measured for  $^{79}\text{Rb}$ .

$E_\gamma$	$I_i \rightarrow I_f$	$a_2$	$a_4$	$\delta$
135.1	$5/2^- \rightarrow 3/2^-$	-0.56(6)	0.07(7)	0.18(12)
147.0	$7/2^+ \rightarrow 5/2^+$	0.05(5)	-0.03(7)	-0.19(10)
500.8	$13/2^+ \rightarrow 9/2^+$	0.35(6)	-0.03(1)	0.0(1)
547.2	$11/2^+ \rightarrow 9/2^+$	0.35(6)	0.13(9)	-0.38(14)

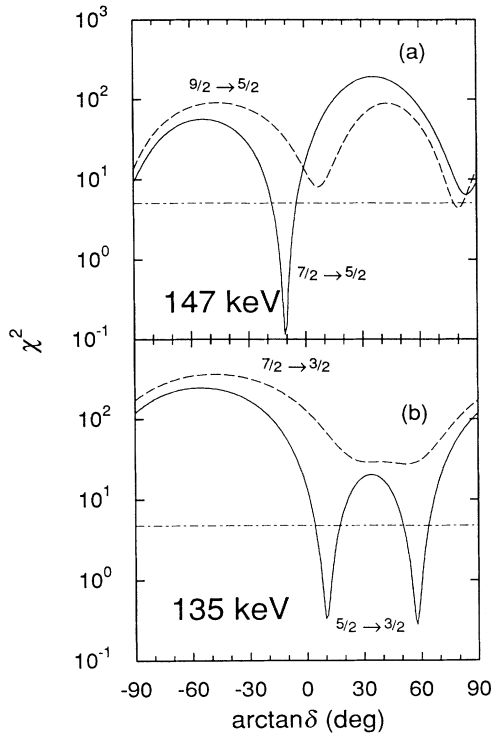


FIG. 4. Graphs of  $\chi^2$  vs  $\arctan(\delta)$  for the 135 and 147 keV transitions. The solid (dashed) line represents  $\chi^2$  calculated for a  $I \rightarrow I - 1$  ( $I \rightarrow I - 2$ ) transition. The dash-dotted line represents the 0.1% confidence limit.

the spin and parity of the 39 keV state in  $^{79}\text{Rb}$  were  $\frac{1}{2}^-$ , then its lifetime of 23(1) ns [20] or 26(1.6) ns [21] would imply an unreasonable large  $B(M2)$  strength of about  $2 \times 10^4$  single particle units. A possible spin-parity of  $\frac{5}{2}^-$  is also ruled out by the lifetimes [6] of the 680 and 1349 keV states and their observed decays to positive-parity states. Their spins are related to the bandhead spin by the measured DCO ratios. A bandhead spin of  $\frac{5}{2}^-$  would imply spins of  $\frac{11}{2}$  and  $\frac{15}{2}$  for the 680 and 1349 keV levels, respectively. The decays of these states to levels in the positive-parity band with transition energies of 533 and 705 keV would then have unreasonably large  $B(M2)$  strengths of 842 and 523 single particle units, respectively.

Therefore, the spin and parity of the 39 keV bandhead state are  $\frac{3}{2}^-$ . A word of caution concerns the spin-parity of the  $^{79}\text{Sr}$  ground state which has been reported [22, 23] without parentheses and on which the present assignment in  $^{79}\text{Rb}$  is based. A spin of  $\frac{3}{2}$  is firmly established [24] for  $^{79}\text{Sr}$ , but the parity assignment is not as clearly established.

An angular distribution was also measured for the 135 keV  $\frac{5}{2}^-$  to  $\frac{3}{2}^-$  transition. Both minima in the  $\chi^2$  graph in Fig. 4 imply positive mixing ratios, in general agreement with the DCO ratio analysis.

#### D. Other negative-parity states

An additional  $\gamma$  decay sequence built on a 144 keV state has been proposed [5], although none of the lines

are in coincidence with any lines in the previously discussed bands. The two lowest states in this cascade were first assigned to  $^{79}\text{Rb}$  in  $\beta$  decay studies [20, 21]. The present observation of an additional pair of  $\gamma$  decays from the 670 keV state whose energy differs by 39 keV (the energy of the first excited state in  $^{79}\text{Rb}$ ) provides additional evidence for the assignment of this band to  $^{79}\text{Rb}$ .

The observation [20, 21] of allowed  $\beta$  decay from the  $\frac{3}{2}^-$  ground state of  $^{79}\text{Sr}$  to the 144 keV state in  $^{79}\text{Rb}$  limits the spin-parity of the latter state to  $\frac{1}{2}^-$ ,  $\frac{3}{2}^-$ , or  $\frac{5}{2}^-$ . A spin of  $\frac{1}{2}$  is ruled out by the DCO ratio of 0.63(15) for the ground state  $\gamma$  decay of this state, which is inconsistent with multipolarity 2 decay. Since the DCO ratio of the 526 keV transition implies  $\Delta I = 2$ , a spin-parity of  $\frac{5}{2}^-$  for the 144 keV state would imply  $\frac{9}{2}^-$  for the 670 keV state and  $M3$  multipolarity for its decay to the  $\frac{3}{2}^-$  39 keV state. However, the mean life of the 670 keV state must be less than 50 ns since there is no loss of coincidence intensity at this state. This would lead to an unreasonably large  $B(M3)$  strength greater than 14 000 single particle units.

Therefore, the spin and parity of the 144 keV state is  $\frac{3}{2}^-$ . Enough DCO ratios could be measured in this more weakly populated band to reliably assign the spins for all but two of the states in this band.

#### E. Higher-lying negative-parity states

In addition to the cascades with low-lying bandhead states, a decay sequence has been observed which is built on a 3309 keV state and consists mainly of  $\Delta I = 1$  transitions. The 3309 keV state decays to both the  $\frac{17}{2}^+$  and the  $\frac{17}{2}^-$  states, and is tentatively assigned a spin and parity of  $(\frac{19}{2}^-)$ . This assignment is based on its similarity to a high-lying 3-qp band in  $^{83}\text{Rb}$  [7]. Due to the weak population of these states, no reliable DCO ratios could be measured for the  $\gamma$  rays. Assignments of transition multiplicities as well as the spins and parities of the states are, therefore, tentative.

#### F. Decay sequence of unknown parity

A gate on the 119 keV line shows clear coincidences with a 54 keV  $\gamma$  ray and with many known transitions in the  $\alpha = +\frac{1}{2}$  band (505, 669, 815, 946, and 1090 keV lines). Intensity relations suggest that the low energy transitions lie at the bottom of the decay sequence and hence imply a new low-lying level at 119 or 54 keV. It is a little surprising that such a state was not seen in the  $\beta$ -decay experiments, but the coincidence relations have been seen clearly in the  $\gamma$ - $\gamma$  coincidence matrices from both reactions. In addition, both matrices show coincidence relationships between the 119, 655, 742, and possibly 841 keV lines. This suggests the existence of a new  $\gamma$  decay sequence in  $^{79}\text{Rb}$  ending on a 119 keV state.

## IV. LIFETIME MEASUREMENTS

Lifetimes for the shorter-lived higher-lying states were extracted via the Doppler-shift attenuation method

(DSAM) using a computer code [16] that simulates the slowing down process of the recoiling nucleus. The stopping powers of Northcliffe and Schilling [25] were scaled [26] to the measured [27]  $\alpha$  stopping powers in  $^{63}\text{Cu}$  at the same velocity. The scaling factor varied from 0.98 to 1.14 over the range of possible recoil energies. The theoretical line shape generated by the simulation process was compared to the measured forward coincidence spectrum, and the lifetime was varied in the simulation to give the best fit. The uncertainty in the lifetime was determined by comparing the accuracy of the best fit lifetime with the accuracy for lifetime fits near the measured best value.

For the highest measurable lifetime in each cascade, only an upper limit for the lifetime can be established due to the inability to correct for the feeding of that state. For all other lifetimes, corrections for direct feeding from in-cascade transitions as well as side-feeding times were made.

For a number of transitions, forward coincidence spectra gated on lines in the  $90^\circ$  detectors from above (GFA) and below (GFB) the transition of interest were used to determine the side-feeding times of the states. For example, Fig. 5 shows spectra generated for the 962.5 keV transition from (a) GFA and (b) GFB. A GFA fit is independent of the side-feeding time of that state. Consequently, for a corresponding GFB spectrum, fits are

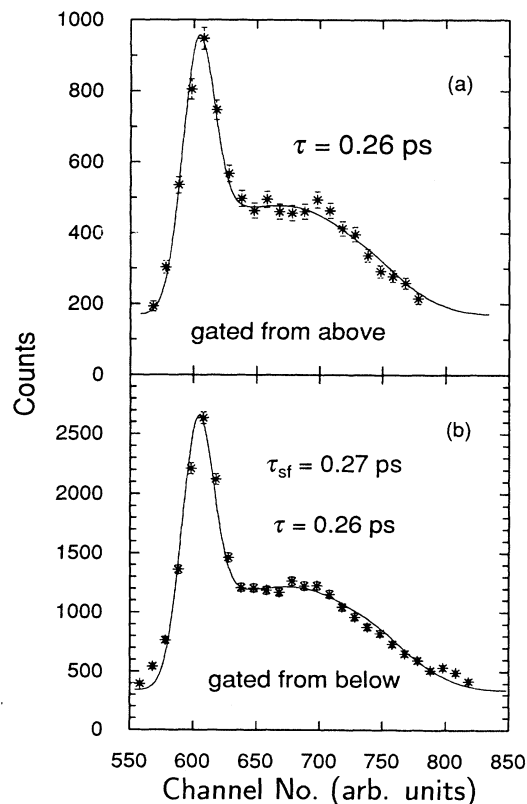


FIG. 5. Doppler shift attenuation fits to the line shapes of the 963 keV transition to determine the lifetime of the  $\frac{21}{2}^+$  state. (a) Spectrum generated by gating from above the 963 keV transition. (b) Spectrum generated by gating from below the 963 keV transition.

made over a range of side-feeding times, keeping all other input parameters the same as in the GFA case. The side-feeding time assigned is that which reproduces the lifetime extracted from the GFA spectrum. Figure 6 shows a plot of  $\chi^2$  as a function of side-feeding time for the  $\gamma$  rays deexciting the  $\frac{25}{2}^+$  and  $\frac{21}{2}^+$  states keeping all other parameters constant. As can be seen, a relatively sharp minimum allows a reasonable assignment of the side-feeding times for those states.

For states for which GFA spectra fits could not be made due to lack of statistics, an alternate method was used. Both the lifetime of the state and the side-feeding time into it were allowed to vary to achieve the best fit. However, because they are not determined as well by this procedure, the side-feeding times were constrained to lie within  $\pm 25\%$  of the curve in Fig. 7 determined by the GFA fits. Although the side-feeding times inferred only from the GFB spectra cannot be considered independent determinations, the good fits obtained show that they are consistent with those determined by the former method. These side-feeding times are close to the lifetimes of the states into which they feed and are similar to the effective lifetimes of the states immediately above.

Present values for mean lifetimes and proposed side-feeding times as well as previously published lifetimes [6] are given in Table III. The somewhat shorter lifetimes reported here are due, at least in part, to the longer side-feeding times used.

The side-feeding times determined in the present work are consistent with those measured [28] recently for  $^{83}\text{Y}$ . A side-feeding time of 0.6 ps was determined for the  $\frac{21}{2}^+$

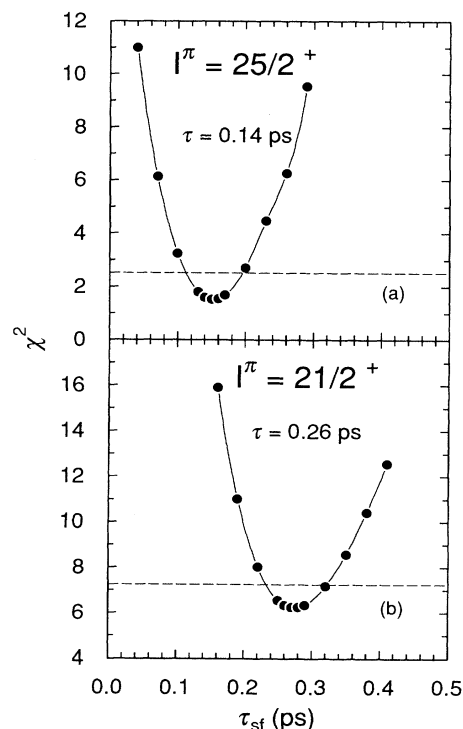


FIG. 6. Graphs of  $\chi^2$  as a function of side-feeding time for (a) the  $\frac{25}{2}^+$  state and (b) the  $\frac{21}{2}^+$  state. The dashed line represents the  $(\chi^2_{\min} + 1)$  level of confidence.

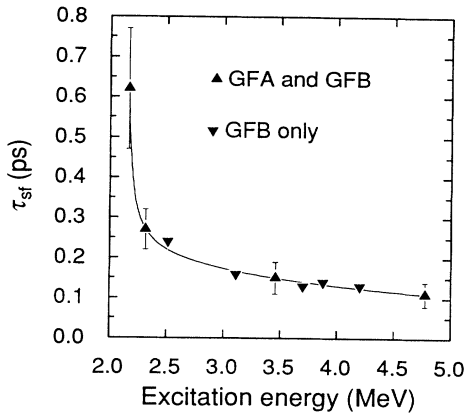


FIG. 7. A plot of side-feeding time vs excitation energy from the DSAM fits for states in  $^{79}\text{Rb}$ . The lifetime of each state was held fixed at the value shown in the figure.

state in  $^{83}\text{Y}$  at 2371 keV by gating from above and below, and side-feeding time limits of  $\leq 0.23$  ps were determined for the  $\frac{25}{2}^+$  and ( $\frac{29}{2}^+$ ) levels at 3450 keV and 4643 keV by assuming a constant quadrupole moment. The increase in side-feeding time with decreasing excitation energy or spin is also consistent with trends [29] previously observed experimentally and simulated theoretically. However, there is a considerable variation in side-feeding times for heavy-ion induced reactions in the literature, and the present values are about a factor of 2 smaller than those reported for  $^{77}\text{Rb}$  [1], but about a factor of 2 larger than those reported for  $^{75}\text{Br}$  [30].

## V. DISCUSSION

### A. Cranked shell model analysis

Band crossings in the positive-parity bands have been discussed previously [5, 31]. The present work confirms the level scheme on which those analyses were based. It was suggested [31] in the analysis of  $^{79}\text{Rb}$  that in rotational bands with very large signature splitting, the unfavored higher-lying signature may be crossed by another band with the same signature and parity but of a different structure. Following this suggestion, a search was made for such states. Due possibly to a lack of statistics, however, none of the states were observed. As will be discussed in Sec. VC the measured  $Q_t$  values are in good agreement with the theoretical calculations and tend to confirm that analysis.

The kinematic moments of inertia  $J^{(1)}$  and Routhians  $e'$  for the negative-parity bands are compared in Fig. 8. The curves of  $J^{(1)}$  for the yrast negative-parity bands increase gently toward the rigid body value. A broad alignment at  $\hbar\omega \approx 0.5$  MeV can be seen in the  $\alpha = +\frac{1}{2}$  curve which is not present in the  $\alpha = -\frac{1}{2}$  curve. The sharp upbend in  $J^{(1)}$  previously observed [5] above 0.7 MeV/ $\hbar$  lies beyond the levels which could be observed in the present experiments. The values of  $J^{(1)}$  in the new negative-parity bands start lower and increase more rapidly. A sharp upbend is seen at the last tentative point. This occurs at about the same frequency as a sharp upbend in the lowest negative-parity band of  $^{81}\text{Rb}$  [2].

TABLE III. Mean lifetimes and side-feeding times measured for states in  $^{79}\text{Rb}$ .

$E_{\text{lev}}$ (keV)	$I^\pi$	$\tau$ (ps)	$\tau^a$ (ps)	$\tau_{\text{accepted}}$ (ps)	$\tau_{\text{sf}}$ (ps)
96.7	$9/2^+$		$(26 \pm 5) \times 10^3$		
597.5	$13/2^+$		11.9(6)	11.9(6)	
643.9	$11/2^+$		8.2(4)	8.2(4)	
1353.2	$17/2^+$	1.0(3)	1.2(2)	1.0(3)	
1454.4	$15/2^+$		1.3(2)	1.3(2)	
2315.7	$21/2^+$	0.26(3) <sup>b</sup>	0.49(10)	0.26(3)	0.27(5)
2510.2	$19/2^+$	0.23(6) <sup>c</sup>		0.23(6)	0.24
3457.5	$25/2^+$	0.14(3) <sup>b</sup>	0.24(6)	0.14(3)	0.15(4)
3699.8	$23/2^+$	0.14(3) <sup>c</sup>		0.14(3)	0.13
4774.3	$29/2^+$	0.06(2) <sup>b</sup>	<0.3	0.06(2)	0.11(4)
4954.2	$27/2^+$	<0.23		<0.23	>0.23
6274.5	$33/2^+$	<0.10		<0.10	
679.9	$9/2^-$		9.3(25)	9.3(25)	
1349.4	$13/2^-$		1.9(4)	1.9(4)	
2165.1	$17/2^-$	0.53(15) <sup>b</sup>	0.75(20)	0.53(15)	0.62(15)
2767.8	$19/2^-$	0.28(7) <sup>b</sup>		0.28(7)	
3111.4	$21/2^-$	0.23(4) <sup>c</sup>	0.35(10)	0.23(4)	0.16
3878.9	( $23/2^-$ )	0.15(3) <sup>c</sup>		0.15(3)	0.14
4202.0	( $25/2^-$ )	0.12(4) <sup>c</sup>	0.2(1)	0.12(4)	0.13
5142.4	( $27/2^-$ )	<0.17		<0.17	
5463.9	( $29/2^-$ )	<0.21		<0.21	

<sup>a</sup>From Ref. [6].

<sup>b</sup>Lifetime determined from GFA spectrum.

<sup>c</sup>Lifetime determined from GFB spectrum.

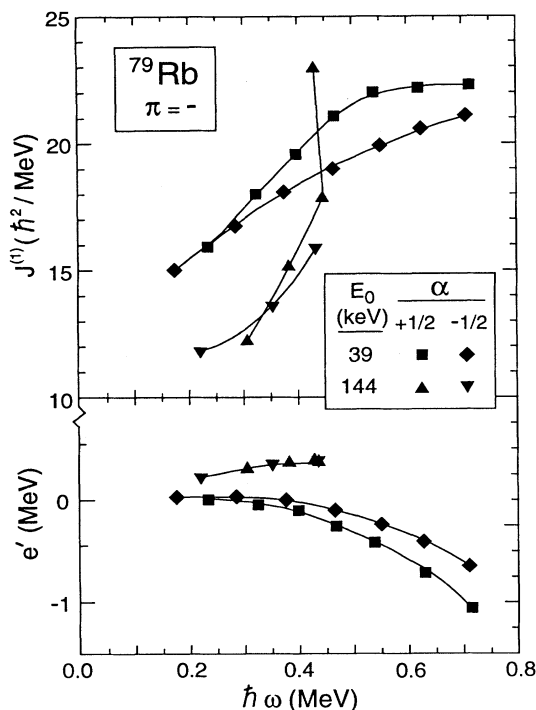


FIG. 8. Kinematic moments of inertia  $J^{(1)}$  and Routhians  $e'$  as a function of rotational frequency  $\hbar\omega$  for the negative-parity bands in  $^{79}\text{Rb}$ . The Harris parameters used for the reference rotor are  $J_0 = 16 \hbar^2 \text{MeV}^{-1}$  and  $J_1 = 1.0 \hbar^4 \text{MeV}^{-3}$ . A  $K$  value of  $\frac{3}{2}$  was used.

The graphs of the Routhians for the yrast negative-parity bands show that the signature splitting increases from about 35 keV to about 300 keV at the highest observed frequency. These rather large values of signature splitting are still considerably smaller than in the positive-parity bands. The splitting in the new negative-parity bands is quite small and reaches only about 20 keV at  $\hbar\omega = 0.43 \text{ MeV}$ , compared to about 100 keV at the same frequency in the yrast bands.

### B. High-lying decay sequence

The  $\gamma$  decay sequence built on the 3309 keV state resembles a structure which has been observed in a number of neighboring odd- $A$  Rb, Kr, and Br isotopes. Some of the characteristics are the high excitation energy, the dominance of  $\Delta I = 1$  transitions, and the decay out of the sequence to both positive- and negative-parity bands. The bandhead spin varies in the Br isotopes from  $(\frac{17}{2}^-)$  ( $^{77}\text{Br}$ ) [10] to  $(\frac{13}{2}^-)$  ( $^{79}\text{Br}$  and  $^{81}\text{Br}$ ) [11, 12]. In  $^{79}\text{Kr}$ , a similar structure starts at  $(\frac{17}{2}^-)$  [32]. A comparison of apparently similar structures in the Rb isotopes is shown in Fig. 9. The spin of the lowest observable state also increases from  $^{83}\text{Rb}$  [7] ( $\frac{13}{2}^-$ ) to  $^{81}\text{Rb}$  [8, 9] ( $\frac{15}{2}^-$ ) to  $^{79}\text{Rb}$  ( $\frac{19}{2}^-$ ).

In  $^{83}\text{Rb}$  a  $[\pi g_{9/2} \otimes \nu g_{9/2} \otimes \nu(pf)]$  3-qp configuration has been proposed [7] for the structure. Pauli blocking argu-

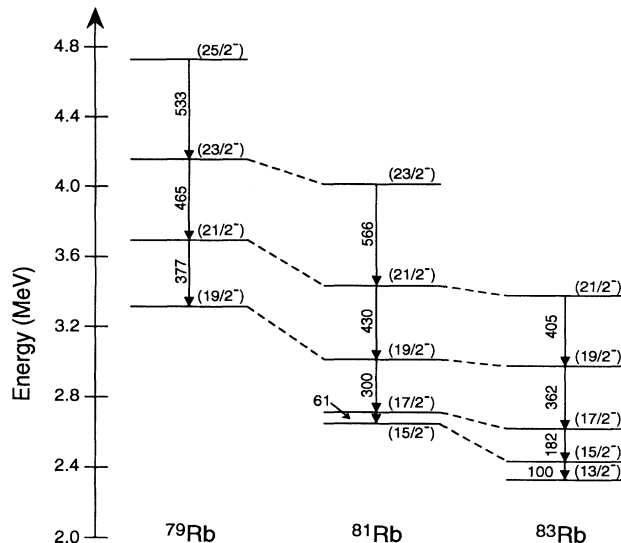


FIG. 9. A comparison of the high-lying 3-quasiparticle bands in neighboring odd Rb isotopes.

ments suggest that a neutron qp pair would be favored in an odd- $Z$  nucleus. Particles in the unique-parity  $g_{9/2}$  orbital would provide much of the high intrinsic spin and a neutron in the  $pf$  orbitals ( $p_{1/2}$ ,  $p_{3/2}$ , or  $f_{5/2}$ ) would provide the negative parity.

Recent deformed shell-model calculations [33] for the Br isotopes may also be relevant for the Rb nuclei. The 3-qp configurations which they considered most likely for a  $K = \frac{13}{2}^-$  band are

- Proton in  $K = \frac{3}{2}^+$  orbit, neutrons in  $K = \frac{5}{2}^+$  and  $\frac{5}{2}^-$  orbits.
- Proton in  $K = \frac{1}{2}^+$  orbit and neutrons in  $K = \frac{7}{2}^+$  and  $\frac{5}{2}^-$  orbits.
- Proton in  $K = \frac{1}{2}^-$  orbit and neutrons in  $K = \frac{5}{2}^+$  and  $\frac{7}{2}^+$  orbits.

The intrinsic state obtained from configuration (a) produced the lowest energy states for  $^{77,79}\text{Br}$ , while the intrinsic state obtained from configuration (c) produced the lowest energy state for  $^{81}\text{Br}$ . The experimentally determined states in  $^{77,79}\text{Br}$  were reasonably reproduced by the deformed shell model calculations, while the agreement in bandhead energy and spacing was not as good in  $^{81}\text{Br}$ . It was found that these three configurations did not mix much with each other or with the low-lying negative-parity bands. This might explain the decay out of the high- $K$  configurations, which does not occur preferentially to lower negative-parity states. A theoretical comparison of the relative  $M1$  and  $E2$  strengths in the low- and high-lying negative-parity bands would be most informative since they differ so much experimentally.

The configuration in  $^{79}\text{Rb}$  is likely to be similar to that in the isotope  $^{77}\text{Br}$ . Therefore, a suggested configuration for the high-lying sequence in  $^{79}\text{Rb}$  would be  $\pi g_{9/2} \otimes$

$\nu_{g_{9/2}} \otimes \nu(pf)$ . Such a combination allows for a spin and parity of  $\frac{13}{2}^-$ , but, as in  $^{77}\text{Br}$ , the band is not observed at such low spin. The lowest proposed spin experimentally observed is  $(\frac{19}{2}^-)$ .

As suggested [33] for  $^{77}\text{Br}$ , a search was made in the coincidence spectra for transitions to extend the 3-qp sequence to states of lower spin and excitation energy, but none were found. The lower-spin states may be present, but not observable under the present conditions, or the decay sequence may be based on a higher  $K$  state. The former is quite possible since the high excitation energy of this structure reduces its population strength and also increases the probability of decay out of the band to low-lying states.

### C. Transition strengths and deformation

Electric quadrupole transition strengths,  $B(E2)$ , have been determined from the accepted lifetimes given in Table III and used to calculate transition quadrupole moments,  $|Q_t|$ , according to the rotational model. An effective value of  $K = \frac{3}{2}$  was used for both the positive- and negative-parity bands. Quadrupole deformations ( $\beta_2$ ) were then inferred, assuming axial symmetry, to give an indication of the amount of nuclear deformation involved. These values are given in Table IV.

Considerable collective enhancement is demonstrated by the high quadrupole transition strengths ranging from about 70 to over 200 single particle units. These transition strengths imply axial deformations ranging from

$\beta_2 = 0.33\text{--}0.44$ , except for the  $\frac{15}{2}^+$  state, whose lifetime was not measured in the present experiment. With an axial deformation averaging approximately 0.38 for the favored signatures and slightly lower for the unfavored,  $^{79}\text{Rb}$  is shown to be one of the more highly deformed rotors in this mass region. Note that the parameters calculated from the decay of the highest state in each cascade serve only as a lower limit for actual values.

An indicator of the amount of deformation without assuming axial symmetry is the transition quadrupole moment  $Q_t$ . The transition quadrupole moments determined from the present work were compared to those predicted by Nazarewicz [3] and Bengtsson *et al.* [31] using the deformed Woods-Saxon cranking model of Ref. [34]. Figure 10 shows a plot of  $Q_t$  vs rotational frequency  $\hbar\omega$  for both experimentally and theoretically determined  $Q_t$  values. Experimentally, a relatively constant value averaging 3.2  $e b$  for the favored sequences and slightly less for the nonfavored is observed. Theoretical  $Q_t$  values were calculated from total Routhian surface (TRS) predictions. As shown, the experimentally determined  $Q_t$ 's are relatively consistent with those implied by the predicted deformations. The largest differences come from the transitions decaying from the  $\frac{15}{2}^+$ ,  $\frac{13}{2}^+$ , and  $\frac{11}{2}^+$  states, whose lifetimes were not measured in the present work.

A sample of TRS plots for the negative-parity states is shown in Fig. 11. At a frequency of 0.296 MeV/ $\hbar$  below the band crossing, the shapes are predicted to be nearly prolate with  $\beta_2 \approx 0.30$  for both signatures. At

TABLE IV. Branching ratios, accepted lifetimes, transition strengths, transition quadrupole moments, and quadrupole deformations for electric quadrupole transitions in  $^{79}\text{Rb}$ .

$I_i^\pi$	BR (%)	$\tau_{\text{acc}}$ (ps)	$B(E2)$ (W.u.)	$ Q_t $ (e b)	$\beta_2^a$
$9/2^+$	100	$(26 \pm 5) \times 10^3$	$68_{11}^{16}$		
$11/2^+$	57	$8.2(4)^b$	$93_2^2$	2.72	0.33
$13/2^+$	100	$11.9(6)^b$	$105_6^6$	2.76	0.33
$15/2^+$	81	$1.3(2)^b$	$72_4^5$	2.22	0.27
$17/2^+$	100	1.0(3)	$164_{38}^{70}$	3.28	0.39
$19/2^+$	100	0.23(6)	$134_{28}^{48}$	2.93	0.35
$21/2^+$	100	0.26(3)	$189_{20}^{25}$	3.43	0.40
$23/2^+$	100	0.14(3)	$122_{22}^{32}$	2.73	0.33
$25/2^+$	100	0.14(3)	$149_{26}^{41}$	3.00	0.36
$27/2^+$	100	$<0.23$	$>57$	$>1.84$	$>0.23$
$29/2^+$	100	0.06(2)	$171_{43}^{85}$	3.18	0.38
$33/2^+$	100	$<0.10$	$>53$	$>1.76$	$>0.22$
$9/2^-$	76	$9.3(25)^b$	$100_{21}^{37}$	3.08	0.37
$13/2^-$	85	$1.9(4)^b$	$135_{24}^{36}$	3.12	0.37
$17/2^-$	97	$0.53(15)$	$206_{45}^{81}$	3.67	0.43
$19/2^-$	100	0.28(7)	$192_{29}^{42}$	3.49	0.41
$21/2^-$	100	0.23(4)	$232_{35}^{49}$	3.81	0.44
$(23/2^-)$	100	0.15(3)	$160_{34}^{58}$	3.13	0.37
$(25/2^-)$	100	0.12(4)	$219_{55}^{110}$	3.64	0.43
$(27/2^-)$	100	$<0.17$	$>74$	$>2.11$	$>0.26$
$(29/2^-)$	100	$<0.21$	$>60$	$>1.89$	$>0.23$

<sup>a</sup> Assuming axial symmetry.

<sup>b</sup> Lifetimes from Ref. [6].

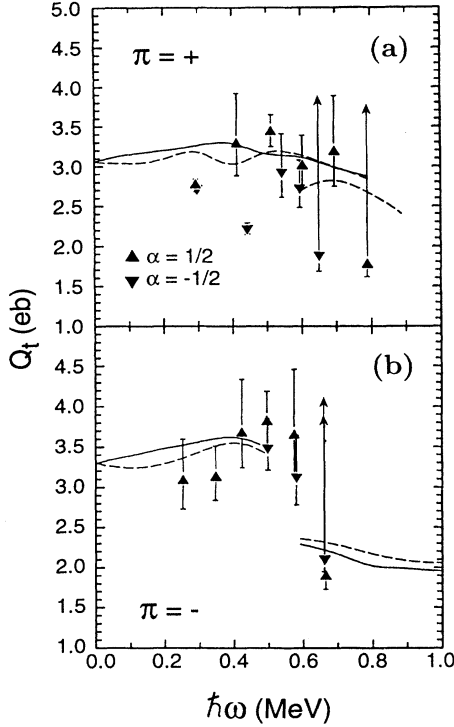


FIG. 10. Transition quadrupole moments  $|Q_t|$  are plotted vs rotational frequency for (a) positive-parity states and (b) negative-parity states in  $^{79}\text{Rb}$ . The solid and dashed curves show the values implied by the shapes predicted for signature  $\alpha = +\frac{1}{2}$  and  $-\frac{1}{2}$ , respectively, by cranking calculations using a deformed Woods-Saxon potential. The two dashed curves in (a) represent two competing shapes.

0.691 MeV/ $\hbar$  above the band crossing, however, highly triaxial shapes ( $\gamma \approx -30^\circ$ ) with  $\beta_2$  slightly above 0.20 are predicted for both signatures. This contrasts with the nearly axially symmetric shape predictions for the positive-parity states above and below the band crossing as shown in the TRS plots of Ref. [31]. These TRS plots show no noticeable drop in  $\beta_2$  at the band crossing but a shift from nearly prolate to nearly oblate in the unfavored signature while the favored signature remains nearly prolate.

#### D. Particle-rotor model calculations

As discussed in Sec. III, the mixing ratios for the  $\Delta I = 1$  transitions in the positive-parity band have been observed to be negative while those in the negative-parity band are positive. This leads to the question of whether the two rotational bands have substantially different shapes. According to Morinaga [35]

$$\delta(M1/E2, IK \rightarrow I-1K) = \frac{(g_K - g_R)}{Q_0} \frac{\sqrt{I^2 - 1}}{0.933E} [1 + \delta_{K,1/2} b_0 (-)^{I+1/2}], \quad (2)$$

where  $Q_0$  (in barns) is the quadrupole moment,  $b_0$  is

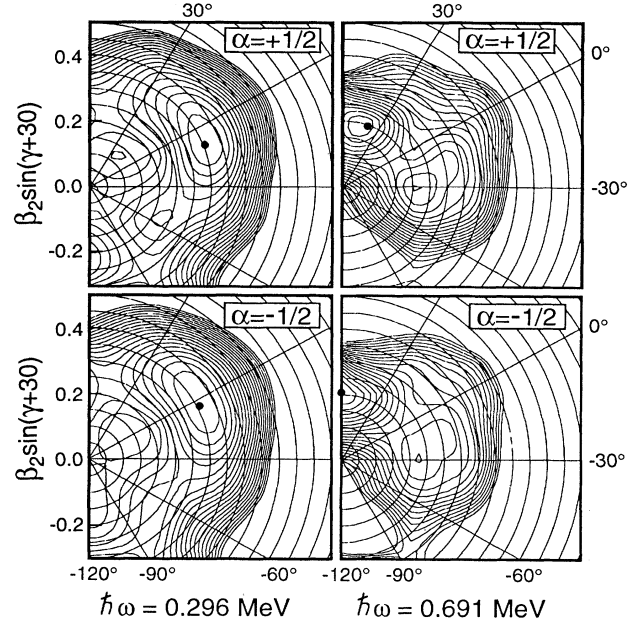


FIG. 11. Total Routhian surfaces in the  $(\beta_2, \gamma)$  polar coordinate plane for negative-parity states with rotational frequencies of  $\hbar\omega = 0.296$  MeV and  $0.691$  MeV for the favored ( $\alpha = +\frac{1}{2}$ ) and unfavored ( $\alpha = -\frac{1}{2}$ ) signatures. The contour lines are in intervals of  $0.25$  MeV.

a term related to the decoupling parameter for  $K = \frac{1}{2}$  bands,  $E$  (in MeV) is the energy of the decaying  $\gamma$  ray, and  $g_K$  and  $g_R$  are the  $g$  factors of the unpaired particle and core, respectively. Qualitatively, the equation above reduces to

$$\text{sgn}(\delta) = \text{sgn} \left( \frac{g_K - g_R}{Q_0} \right). \quad (3)$$

Using the Schmidt limit attenuated by a factor of 0.7 [36] gives  $g_K$  values of 1.32 and 1.97 for a  $g_{9/2}$  or  $p_{3/2}$  proton. Both of these values are considerably larger than the core  $g$  factor  $g_R \approx Z/A = 0.47$ , so the numerator in Eq. (3) ( $g_K - g_R$ ) is positive for both bands. This would imply a negative quadrupole moment  $Q_0$  and an oblate shape for the positive-parity band in contradiction with the predictions of the Hartree-Fock-Bogolyubov cranking calculations. However, Eq. (2) is based on the strong-coupling approximation and may not be applicable to the positive-parity band which shows strong signature splitting.

We have performed particle-rotor model calculations to resolve this question. The codes GAMPN, ASYRMO, and PROBAMO [37, 38] were used with standard parameters [39] for the modified harmonic oscillator potential. A variable moment of inertia was used for the rotor with the Harris parameters  $J_0 = 15\hbar^2/\text{MeV}$  and  $J_1 = 10\hbar^4/\text{MeV}^3$  which were fitted to the neighboring even-even nuclei,  $^{78}\text{Kr}$  and  $^{80}\text{Sr}$ . The shapes predicted by the Hartree-Fock-Bogolyubov cranking calculations for a rotational frequency of  $0.3$  MeV/ $\hbar$  were used (see Fig. 11). The resulting deformations after trans-

formation from the Woods-Saxon to the modified oscillator parametrization were  $\epsilon_2 = 0.299$ ,  $\gamma = 6.8^\circ$ , and  $\epsilon_4 = 0.044$  for the positive-parity states and  $\epsilon_2 = 0.321$ ,  $\gamma = 2.7^\circ$ , and  $\epsilon_4 = 0.031$  for the negative-parity states. These slightly different shapes were the only parameters which differed for the calculations of the two parities, but the results would not have been significantly different if a single average shape had been used for all the states. A Coriolis attenuation factor of  $\xi = 0.7$  was used for all the calculations.

The 1-qp excitation energies predicted by the particle-rotor calculation are compared with the experimentally observed ones in Fig. 12. The level ordering and different degrees of signature splitting are predicted well by the calculations. The overall agreement is excellent for the negative-parity band, while the energies of the high-spin positive-parity states are underpredicted by about 20%. However, the qualitative features are reproduced quite well. The close spacing between the  $\frac{5}{2}^+$  and  $\frac{9}{2}^+$  states is predicted, as is the relative position of the unfavored signature states above those of favored signature and lower spin.

The good agreement in Fig. 12 suggests that the 1-qp states in these bands (before the alignment discussed

in Sec. V A) are rather well described by the calculations, and an examination of the predicted mixing ratios  $\delta$  would be instructive. Some of the calculated mixing ratios in the positive-parity band are  $-0.17$  for the  $\frac{7}{2}^+ \rightarrow \frac{5}{2}^+$  transition and  $-0.38$  for the  $\frac{11}{2}^+ \rightarrow \frac{9}{2}^+$  transition. These are in excellent agreement with the measured ones in Table II and prove that the observed values are consistent with the predicted prolate shape for the positive-parity band. In the negative-parity band mixing ratios of 1.13, 1.23, and 1.17 are predicted for the  $\frac{5}{2}^- \rightarrow \frac{3}{2}^-$ ,  $\frac{7}{2}^- \rightarrow \frac{5}{2}^-$ , and  $\frac{9}{2}^- \rightarrow \frac{7}{2}^-$  transitions. These large positive values are in qualitative agreement with the very small DCO ratios measured in this band, although the first value is much larger than that listed in Table II.

The particle-rotor calculations also predict a low-lying  $\frac{3}{2}^+$  state at 212 keV. It is possible that this state corresponds to the one measured at 119 keV. Positive parity for this state would explain why it was not seen in the  $\beta$  decay experiments, but neither the spin nor the parity have been determined experimentally.

The calculations predict a second negative-parity band based on a  $\frac{5}{2}^-$  bandhead. The predicted energies agree rather well with those in the other negative-parity band, which includes the 363 keV  $\frac{5}{2}^-$  state. However, there is no predicted analog of the 144 keV  $\frac{3}{2}^-$  state. Another possibility for this band is suggested by the coexisting oblate shape predicted in Fig. 11. Particle-rotor calculations for this shape ( $\epsilon_2 = -0.23$ ,  $\gamma = 0^\circ$ ) predict a low-lying  $K^\pi = \frac{3}{2}^-$  band, but with a significant degree of signature splitting. Some degree of triaxiality might bring this into better agreement with experiment.

The present particle-rotor model calculations can be compared with earlier calculations for the positive-parity yrast bands of  $^{79}\text{Rb}$  [6] and  $^{81}\text{Rb}$  [40] with a relatively similar asymmetric rotor model [41] and with the interacting-boson-fermion model [42]. The level schemes predicted by both models are relatively close to the experimental ones and to the present calculations. All the calculations predict very large signature splitting with inverted level ordering, as observed. The energy levels calculated in Refs. [6, 40] are not as depressed as in Fig. 12, but more parameters were adjusted. In the asymmetric rotor calculations, which were made for a large triaxiality of  $\gamma = 27^\circ$ , the degree of depression depended on  $\beta_2$  and was smallest for a rather large value of  $\beta_2 = 0.42$ . In general, one can conclude that both the particle-rotor and interacting-boson-fermion models are capable of reproducing the somewhat unusual inverted level ordering found in  $^{79,81}\text{Rb}$ .

## VI. SUMMARY

Two fusion-evaporation reactions were used to study the high-spin states of  $^{79}\text{Rb}$ . On the basis of  $\gamma$ - $\gamma$  coincidence measurements a level scheme has been established. DCO ratios and an angular distribution measurement were used to assign spins and parities for many of the states. The Doppler-shift attenuation method was used to determine the lifetimes of many of the positive-

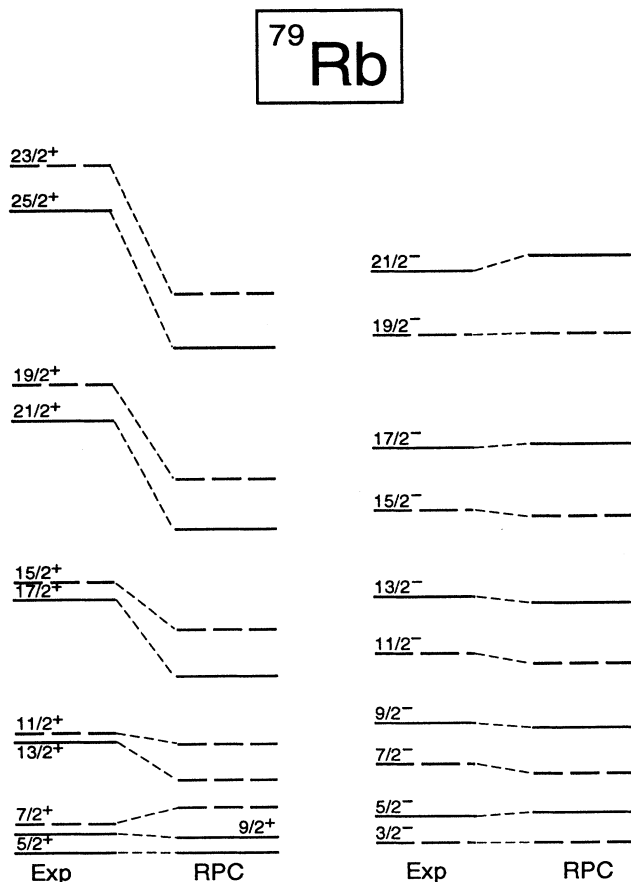


FIG. 12. A comparison of 1-qp excitation energies predicted by the particle-rotor model (RPC) with those measured experimentally.

and negative-parity states. Side-feeding times were determined directly by comparing line shapes fitted from spectra gated from above and below the transition of interest. Large quadrupole deformations were observed with  $\beta_2$  ranging from 0.33 to 0.44 (assuming axial symmetry), showing that the shape of  $^{79}\text{Rb}$  lies between that of  $^{77}\text{Rb}$  and  $^{81}\text{Rb}$ . Values for the transition quadrupole moments deduced from the lifetimes agree well with those predicted by a deformed Woods-Saxon calculation. Particle-rotor model calculations using these predicted shapes account rather well for the 1-qp energy spacings observed in the lower-lying part of these bands and for the differences in the signs of the mixing ratios.

Further evidence was found to support the assignment of a rotational band built on a  $\frac{3}{2}^-$  level at 39 keV to  $^{79}\text{Rb}$ . A new state at 119 keV and several members of a  $\gamma$  decay

cascade built on it have been observed. Also, a new group of states consisting of relatively strong  $\Delta I = 1$  transitions built on a  $(\frac{19}{2}^-)$  state at 3309 keV has been established. This group is strikingly similar to many others found in neighboring odd-*A* Rb and Br isotopes and is interpreted as a 3-qp band with the configuration  $[\pi g_{9/2} \otimes \nu g_{9/2} \otimes \nu(pf)]$ .

#### ACKNOWLEDGMENTS

This work was supported in part by the National Science Foundation. We wish to thank W. Nazarewicz for providing his Hartree-Fock-Bogolyubov cranking calculations. We are grateful to P. Semmes for informative discussions and to P. Semmes and I. Ragnarsson for providing the particle-rotor codes used.

- 
- [1] L. Lühmann, K.P. Lieb, C.J. Lister, B.J. Varley, J.W. Olness, and H.G. Price, *Europhys. Lett.* **1**, 623 (1986).
  - [2] S.L. Tabor, P.D. Cottle, C.J. Gross, U.J. Hüttmeier, E.F. Moore, and W. Nazarewicz, *Phys. Rev. C* **39**, 1359 (1989).
  - [3] W. Nazarewicz (private communication).
  - [4] S.L. Tabor, *Phys. Rev. C* **34**, 311 (1986).
  - [5] Ö. Skeppstedt, C.J. Lister, A.A. Chishti, B.J. Varley, W. Gelletly, U. Lenz, R. Moscrop, and L. Goettig, *Nucl. Phys.* **A511**, 137 (1990).
  - [6] J. Panqueva, H.P. Hellmeister, L. Lühmann, F.J. Bergmeister, K.P. Lieb, and T. Otsuka, *Nucl. Phys.* **A389**, 424 (1982).
  - [7] W. Gast, K. Dey, A. Gelberg, U. Kaup, F. Paar, R. Richter, K.O. Zell, and P. von Brentano, *Phys. Rev. C* **22**, 469 (1980).
  - [8] W. Wagner, L. Funke, J. Döring, L. Käubler, R. Schwengner, and G. Winter, *Rosendorf Annual Report No. ZFK-667*, 28 (1989).
  - [9] H. Rotter, J. Döring, L. Funke, L. Käubler, R. Schwengner, and G. Winter, *Rosendorf Annual Report, No. FZR 93-10*, 81 (1993).
  - [10] J. Döring, L. Funke, R. Schwengner, and G. Winter, in *Nuclear Structure in the Nineties*, edited by N. Johnson (Oak Ridge, Tennessee, 1990), p. 84.
  - [11] R. Schwengner, J. Döring, L. Funke, H. Rotter, G. Winter, A. Johnson, and A. Nilsson, *Nucl. Phys.* **A486**, 43 (1988).
  - [12] L. Funke, J. Döring, P. Kemnitz, P. Ojeda, R. Schwengner, E. Will, G. Winter, A. Johnson, L. Hildingsson, and Th. Lindblad, *Z. Phys. A* **324**, 127 (1986).
  - [13] S.L. Tabor, *Nucl. Instrum. Methods* **A265**, 495 (1988).
  - [14] S.L. Tabor, M.A. Riley, J. Döring, P.D. Cottle, R. Books, T. Glasmacher, J.W. Holcomb, J. Hutchins, G.D. Johns, T.D. Johnson, T. Petters, O. Tekyi-Mensah, P.C. Womble, L. Wright, and J.X. Saladin, *Nucl. Instrum. Methods, Phys. Res. B* **79**, 821 (1993).
  - [15] J.S. Clements, L.R. Medsker, L.H. Fry, Jr., L.V. Theisen, and L.A. Parks, *Phys. Rev. C* **20**, 164 (1979).
  - [16] E.F. Moore, P.D. Cottle, C.J. Gross, D.M. Headly, U.J. Hüttmeier, S.L. Tabor, and W. Nazarewicz, *Phys. Lett. B* **211**, 14 (1988).
  - [17] P. Taras and B. Haas, *Nucl. Instrum. Methods* **123**, 73 (1975).
  - [18] C. Ekström, S. Ingelman, G. Wannberg, and M. Skarestad, *Nucl. Phys.* **A311**, 269 (1978).
  - [19] J. Lipták and J. Křištiak, *Nucl. Phys.* **A311**, 421 (1978).
  - [20] C.J. Lister, P.E. Haustein, D.E. Alburger, and J.W. Olness, *Phys. Rev. C* **24**, 260 (1981).
  - [21] S. Della Negra, H. Gauvin, D. Jacquet, and Y. Le Beyec, *Z. Phys. A* **307**, 305 (1982).
  - [22] C.J. Lister, B.J. Varley, H.G. Price, and J.W. Olness, *Phys. Rev. Lett.* **49**, 308 (1982).
  - [23] J. Heese, K.P. Lieb, S. Ulbig, B. Wörmann, J. Billowes, A.A. Chishti, W. Gelletly, C.J. Lister, and B.J. Varley, *Phys. Rev. C* **41**, 603 (1990).
  - [24] F. Buchinger, E.B. Ramsay, R.E. Silverans, P. Lievens, E. Arnold, W. Neu, R. Neugart, K. Wendt, G. Ulm, and the ISOLDE Collaboration, *Z. Phys. A* **327**, 361 (1987).
  - [25] L.C. Northcliffe and R.F. Schilling, *Nucl. Data Sec. A* **7**, 233 (1970).
  - [26] D. Ward, J.S. Forster, H.R. Andrews, I.U. Mitchell, G.C. Ball, W.G. Davies, and G.J. Costa, *Atomic Energy of Canada Limited, Report No. AECL-5313*, 1976.
  - [27] J.F. Ziegler and W.K. Chu, *At. Data Nucl. Data Tables* **13**, 463 (1974).
  - [28] F. Cristancho, K.P. Lieb, J. Heese, C.J. Gross, W. Fieber, Th. Osipowicz, S. Ulbig, K. Bharuth-Ram, S. Skoda, J. Eberth, A. Dewald, and P. von Brentano, *Nucl. Phys.* **A501**, 118 (1989).
  - [29] F. Cristancho and K.P. Lieb, *Nucl. Phys.* **A486**, 353 (1988).
  - [30] L. Lühmann, M. Debray, K.P. Lieb, W. Nazarewicz, B. Wörmann, J. Eberth, and T. Heck, *Phys. Rev. C* **31**, 828 (1985).
  - [31] R. Bengtsson, W. Nazarewicz, Ö. Skeppstedt, and R. Wyss, *Nucl. Phys.* **A528**, 215 (1991).
  - [32] R. Schwengner, J. Döring, L. Funke, G. Winter, A. Johnson, and W. Nazarewicz, *Nucl. Phys.* **A509**, 550 (1990).
  - [33] R. Sahu and S.P. Pandya, *Nucl. Phys.* **A529**, 20 (1991).
  - [34] W. Nazarewicz, J. Dudek, R. Bengtsson, T. Bengtsson, and I. Ragnarsson, *Nucl. Phys.* **A435**, 397 (1985).
  - [35] H. Morinaga and T. Yamazaki, in *In-Beam Gamma Ray Spectroscopy* (North-Holland, Amsterdam, 1976), p. 159.
  - [36] S. Frauendorf, *Phys. Lett.* **100B**, 219 (1981).
  - [37] S.E. Larsson, G. Leander, and I. Ragnarsson, *Nucl. Phys.* **A307**, 189 (1978).
  - [38] Paul B. Semmes and Ingemar Ragnarsson, in *High Spin*

- Physics and Gamma-Soft Nuclei*, edited by J.X. Saladin, R.A. Sorensen, and C.M. Vincent (World Scientific, Singapore, 1990), p. 500.
- [39] T. Bengtsson and I. Ragnarsson, Nucl. Phys. **A436**, 14 (1985).
- [40] J. Panqueva, H.P. Hellmeister, L. Lühmann, K.P. Lieb, F.J. Bergmeister, P. von Brentano, and R. Richter, Nucl. Phys. **A376**, 367 (1982).
- [41] H. Toki and A. Faessler, Phys. Lett. **63B**, 121 (1976).
- [42] F. Iachello and O. Scholten, Phys. Rev. Lett. **43**, 679 (1979).